



저작자표시-비영리-변경금지 2.0 대한민국

이용자는 아래의 조건을 따르는 경우에 한하여 자유롭게

- 이 저작물을 복제, 배포, 전송, 전시, 공연 및 방송할 수 있습니다.

다음과 같은 조건을 따라야 합니다:



저작자표시. 귀하는 원저작자를 표시하여야 합니다.



비영리. 귀하는 이 저작물을 영리 목적으로 이용할 수 없습니다.



변경금지. 귀하는 이 저작물을 개작, 변형 또는 가공할 수 없습니다.

- 귀하는, 이 저작물의 재이용이나 배포의 경우, 이 저작물에 적용된 이용허락조건을 명확하게 나타내어야 합니다.
- 저작권자로부터 별도의 허가를 받으면 이러한 조건들은 적용되지 않습니다.

저작권법에 따른 이용자의 권리는 위의 내용에 의하여 영향을 받지 않습니다.

이것은 [이용허락규약\(Legal Code\)](#)을 이해하기 쉽게 요약한 것입니다.

[Disclaimer](#)

Thesis for the Degree of Master of Science

Efficiency Enhancement in GaN LED using Nanofeatures by Means of FDTD Simulation



by

ByeongChan Park

Department of physics

The Graduate School

Pukyong National University

February 2015

Efficiency Enhancement in GaN LED using Nanofeatures by Means of FDTD Simulation

(FDTD 시뮬레이션을 이용한
나노구조물을 엮은 GaN LED 의 효율
향상에 대한 연구)

Advisor : Prof. Jae-Won Jang

by

ByeongChan Park

A thesis submitted in partial fulfillment of the requirements

for the degree of Master of Science

in Department of Physics, The Graduate School,

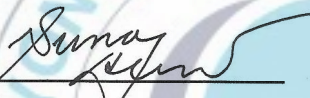
Pukyong National University

February 2015

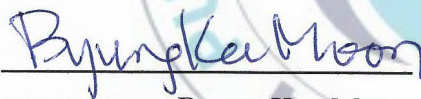
Efficiency Enhancement in GaN LED using Nanofeatures by Means of FDTD Simulation

A dissertation
by
ByeongChan Park

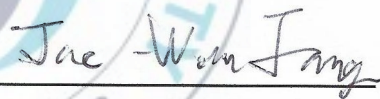
Approved by



(Chairman) Sung Heum Park



(Member) Byung Kee Moon



(Member) Jae-Won Jang

February 27, 2015

Table of contents

Abstract	v
I. Introduction	1
II. Experimental Section	13
III. Results and Discussion	17
3.1 LEE enhancement	17
3.2 Poynting vector intensity: xz view above the GaN layer.....	26
3.3 Poynting vector intensity: xy view and far-field	30
IV. Conclusion	40
V. Reference	41

Figure List

Figure 1.1. Schematic illustration of V-LEDs fabricated with an Al ₂ O ₃ current blocking layer.....	1
Figure 1.2. Schematic side view of the simulated microsphere LED device, and the corresponding SEM images of 100-nm-SiO sphere arrays	2
Figure 1.3. A schematic diagram of power-chip LED structure with sidewall roughness	3
Figure 1.4. Schematic of vertical LEDs with cone-shaped nanostructured surfaces	3
Figure 1.5. Schematic illustrations of fabrication procedures for disordered antireflective nanostructures on GaN-based light-emitting diodes	4
Figure 1.6. Escape cone of an LED without and with encapsulation & Light-extraction efficiency ratio for GaN and GaP as a function of the encapsulant refractive index	4
Figure 1.7. Schematic illustration of the fabrication process for GaN LED with compound eye structures	5
Figure 1.8. Light emission efficiency in GaN calculated for different nonequilibrium carrier concentrations and the PL intensity as a function of dislocation density	6
Figure 1.9. Schematic LED structure with the 3-D- colloidal-phonic-crystal bottom reflector proposed in our study & SEM surface images of colloidal-phonic-crystals fabricated at 30 °C show that the spheres stack with a well-organized (111) plane and fcc structure	7

Figure 1.10. Optical microscopy photo of the fabricated colloidal crystal monolayer and its simulation result	7
Figure 1.11. Oblique-view SEM images of the monolayer hexagonal close-packed polystyrene nanospheres fabricated SiC nanodome structures, and Si ₃ N ₄ coated nanodome structures respectively. A photograph of SiC sample with a partially plain surface and partially covered by the coated nanodome structures	8
Figure 1.12. Schematic diagrams of fabrication process for nanotextured freestanding flip-chip LEDs	9
Figure 1.13. Cross-sectional scheme of an In ₂ O ₃ nano-cones films/GaN-based LED	9
Figure 1.14. Tapping mode AFM topographic images of the PEG nanoscale lenses generated by DPN. Lens size is dependent upon tip-substrate dwell time: 15 s, 10 s, 5 s, and 1 s. The PEG MW was 100000 Da	11
Figure 1.15. Scheme of procedure of ZrO ₂ NP patterning with a wettability tuning method	11
Figure 2.1. Yee algorithm to yield E-field and H-field	13
Figure 2.2. Schemes for 3-D FDTD simulation structures of PEG film and lens or particle addressed GaN LED	14
Figure 3.1. Normalized enhancement of LEE along the normal axis of the GaN LED surface	19
Figure 3.2.1. The top monitor transmittance ratio of the nanomaterials addressed GaN LEDs	21

Figure 3.2.2. $ P_{xz} $ and $ P_{yz} $ of bare GaN LED: (a) xz -view (at $y = 0$) and (b) yz -view (at $x = 0$) of intensity (log scale) of Poynting vector above GaN layer of the bare GaN LED	25
Figure 3.3.1. $ P_{xz} $: xz -view (at $y = 0$) of intensity (log scale) of Poynting vectors above the GaN layer of the nanomaterials addressed LEDs	26
Figure 3.3.2. $ P_{yz} $: yz -view (at $x = 0$) of intensity (log scale) of the Poynting vectors above the GaN layer of the nanomaterials addressed LEDs	27
Figure 3.4. Intensity at the top monitor ($ P_{xy} $, left) and far-field distribution ($ P_{Far} $, right) of Poynting vector with $D = 100\text{nm}$ nanofeatures	33
Figure 3.5. Intensity at the top monitor ($ P_{xy} $, left) and far-field distribution ($ P_{Far} $, right) of Poynting vector with $D = 200\text{nm}$ nanofeatures	34
Figure 3.6.1. Intensity at the top monitor ($ P_{xy} $, left) and far-field distribution ($ P_{Far} $, right) of Poynting vector with $D = 300\text{nm}$ nanofeatures	35
Figure 3.6.2. Intensity at the top monitor ($ P_{xy} $, left) and far-field distribution ($ P_{Far} $, right) of Poynting vector with $D = 400\text{nm}$ nanofeatures	37
Figure 3.6.3. Intensity at the top monitor ($ P_{xy} $, left) and far-field distribution ($ P_{Far} $, right) of Poynting vector with $D = 500\text{nm}$ nanofeatures	38

FDTD 시뮬레이션을 이용한 나노구조물을 엮은 GaN LED의 효율 향상에 대한 연구

박병찬

부경대학교 대학원 물리학과

요약

1990년 대 GaN blue LED가 개발된 이래 관련 연구분야에서는 GaN blue LED의 물리적 특성과 공학적인 응용성의 연구에 초점을 맞추어왔다. LED의 효율에는 내부양자효율 (Internal quantum efficiency), 주입효율 (Injection efficiency), 전기효율 (Electric efficiency) 등이 존재하나 광학적인 관점에서는 광효율 (Light extraction efficiency)에 그 중점을 둔다. LED를 구성하는 물질의 고유한 물성과 관련되어 있는 다른 효율들과는 달리, LED의 광효율은 LED의 발광특성과 관련이 있다. LED는 광학적으로 Incoherent한 면광원이기에 LED 내부에서 생성되어 LED의 표면에 임계각 (GaN: 24°) 이상의 각도로 입사한 광자는 스넬의 법칙에 따라 전반사되어 LED 외부로 방출되지 못한다. 그러나 근래에 들어 이를 micron scale 혹은 nanoscale의 구조물을 이용하면 적지 않은 수의 광자가 임계각을 극복하여 LED 외부로 방출되는 현상들이 보고되었으며 이에 본 연구실에서는 nanoscale의 나노구조물이 Multiple Quantum Wells GaN LEDs 구조에 엮어져 있을 경우 LED 구조의 광효율과 광학적 특성이 어떻게 변화하는지를 시뮬레이션 프로그램을 통하여 알아보고자 하였다.

이를 위하여 3D Finite-Different Time-Domain (FDTD) 프로그램을 이용하여 나노구조물들이 엮어진 Gallium Nitride (GaN) light-emitting device (LED)의 light extraction efficiency를 향상시키는 연구를 수행하였다. 본 연구에서 GaN LED의 Top에 엮어진 나노구조물들은 light extraction layer로 쓰였다.

나노구조물을 구성할 물질의 종류로는 향후의 실험적 구현을 가정하여 구형, 반구형, 그리고 박막 형태의 Polyethylene glycol (PEG)과 구형의 Zirconia (ZrO_2)를 선택하였다. Subwavelength scale 과 over-wavelength scale 의 나노구조물이 얹어진 GaN LED 에 대한 FDTD 시뮬레이션을 수행하여 우리는 각각의 LED 구조의 Poynting vector intensity 의 분포에 대한 정보를 비롯하여 각각의 LED 의 효율과 그 산란 특성 등의 광학적 현상이 어떠한 방식으로 일어나는지를 연구하였다.



I. Introduction

Many experimental methods have been developed to enhance efficiency of LEDs including the first blue-color-emitting GaN LED that was developed in 1994.¹ Especially, the efficiency of GaN LEDs is generally improved in three-different ways composing wall-plug efficiency: Increasing the injection efficiency, internal quantum efficiency (IQE), and light extraction efficiency (LEE)²⁻⁷. They used periodic arrayed nanostructures in GaN LEDs to raise wall-plug efficiency by reduce the photons which are reflected into the interior of the GaN LEDs structure²⁻⁵ and the other authors used periodic arrayed nanostructures on GaN LEDs to use effect of photonic crystal⁶⁻⁷.

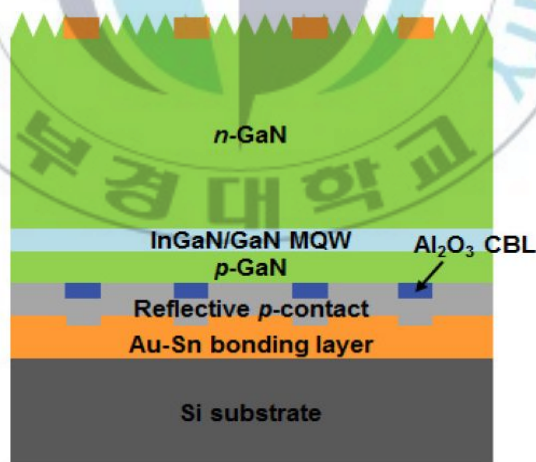


Figure 1.1. Schematic illustration of V-LEDs fabricated with an Al₂O₃ current blocking layer. [3]

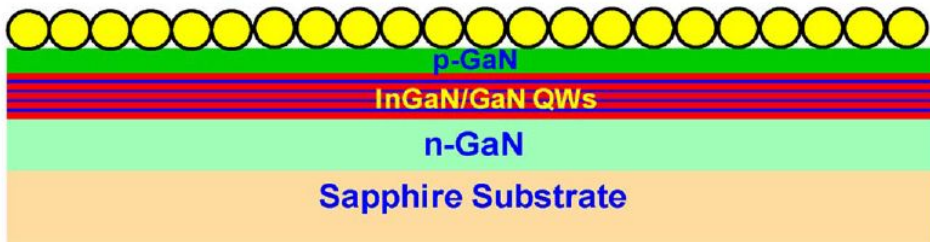


Figure 1.2. Schematic side view of the simulated microsphere LED device, and the corresponding SEM images of 100-nm-SiO sphere arrays. [6]

In the case of injection efficiency and IQE, the number of injected charges (holes and electrons) and the number of excitons (electron-hole pairs) determines the efficiency of the GaN LED. While the number of injected charges and generated excitons are respectively limited by the geometric factors of the LED device and its band structure, the LEE of GaN LEDs is relatively convenient to improve. This is because incrementing the critical angle of the photons escaping from the GaN LED structure is relatively easier than changing the electric properties of the materials composing GaN LED structure. Many ways have been developed and tried to improve the LEE of GaN LEDs, such as surface roughness control by chemical etching ⁸, placing a photonic crystal on top of LED ⁹⁻¹², antireflection coating ¹³, and encapsulation by a high-refractive-index material ^{14,15}. LEE can also be improved by using micro/nanostructures; if subwavelength structures are placed on top of GaN LED, Fresnel reflection decreases, because the reflective index of GaN is gradually matched to that of air by the micro/nanostructures ^{13,16-20}.

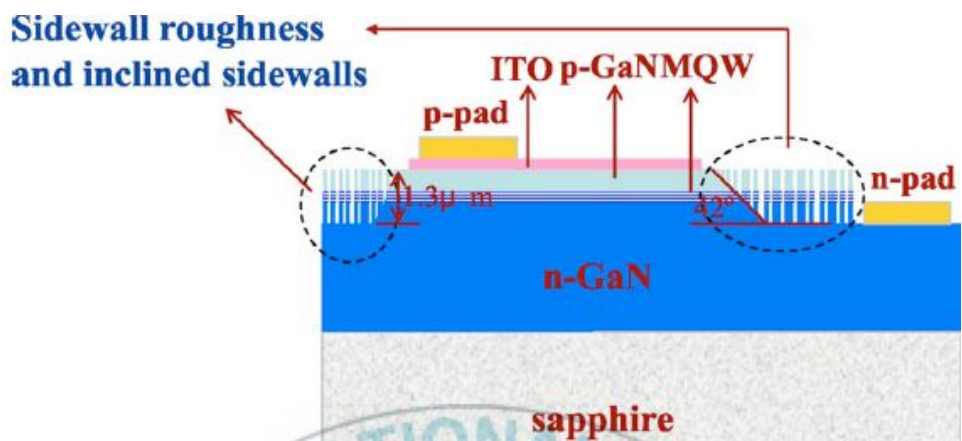


Figure 1.3. A schematic diagram of power-chip LED structure with sidewall roughness. [8]

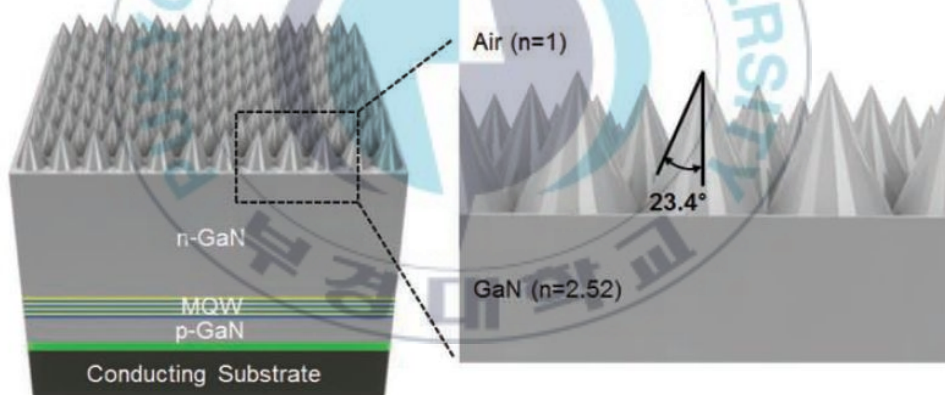


Figure 1.4. Schematic of vertical LEDs with cone-shaped nanostructured surfaces. [9]

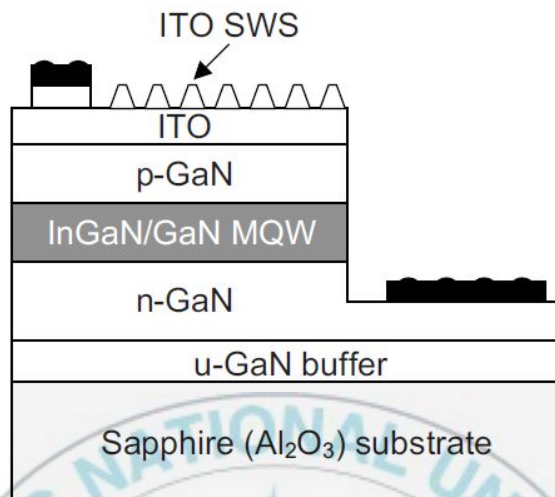


Figure 1.5. Schematic illustrations of fabrication procedures for disordered antireflective nanostructures on GaN-based light-emitting diodes. [13]

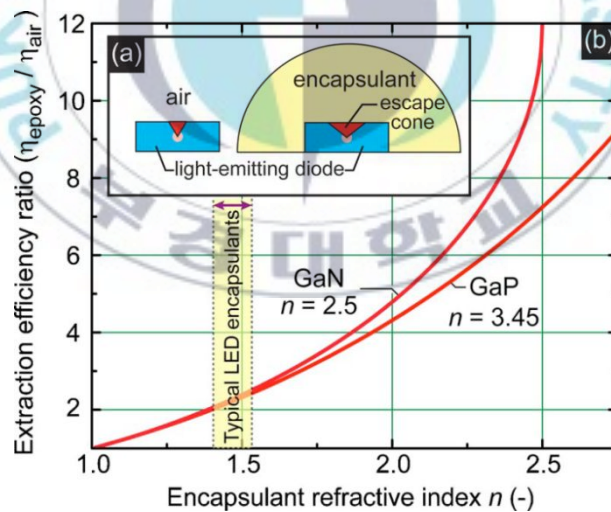


Figure 1.6. (a) Escape cone of an LED without and with encapsulation. (b) Light-extraction efficiency ratio for GaN and GaP as a function of the encapsulant refractive index.

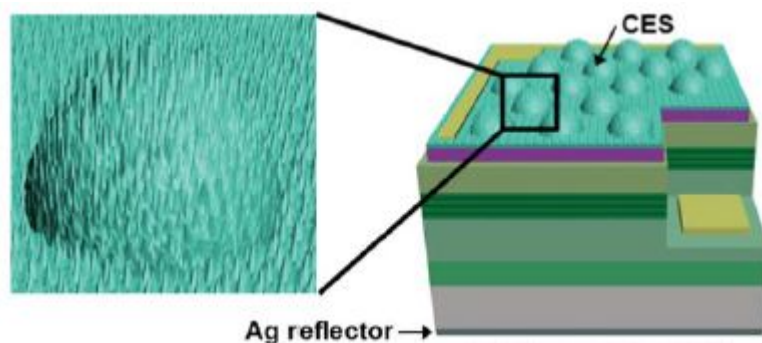


Figure 1.7. Schematic illustration of the fabrication process for GaN LED with compound eye structures. [20]

Most methods for improving LEE have drawbacks as well as advantages in their real application in a device. In the case of the surface roughening of the GaN layer placed on top of LED structure by chemical etching, the dislocation of the GaN layer, which reduces the IQE of the LED, can occur during the chemical etching process.²¹⁻²⁴ Photonic crystals made by micro/nanostructures can utilize optical guided modes for enhancement of LEE due to its periodic structures;^{4,25-30} for examples, SiO₂ photonic crystal was embedded into GaN/InGaN LED using hologram lithography and reactive ion etching (RIE),⁴ auto-cloned photonic crystal²⁶ and colloidal photonic crystal³⁰ were used as bottom reflector of GaN LED, and spherical oxide photonic crystals were fabricated on top layer of GaN LED^{27,29}. In addition, it is reported that LEE can be improved by both plasmonic mode and guided mode in metallo-dielectric³¹ and hetero-dielectric photonic crystals^{32,33}. However, the fabrication of highly ordered structures in a large area on top of GaN LED is challenging. A top-down approach for the mass

fabrication of the ordered structures cannot be free from the chemical or photochemical etching process.^{8,34-36} Moreover, subwavelength-scaled high-refractive-index materials can increase the critical angle of the photons generated in the GaN LED^{14,27,37,38}, but hybrid structures on the GaN layer cannot be conveniently obtained.

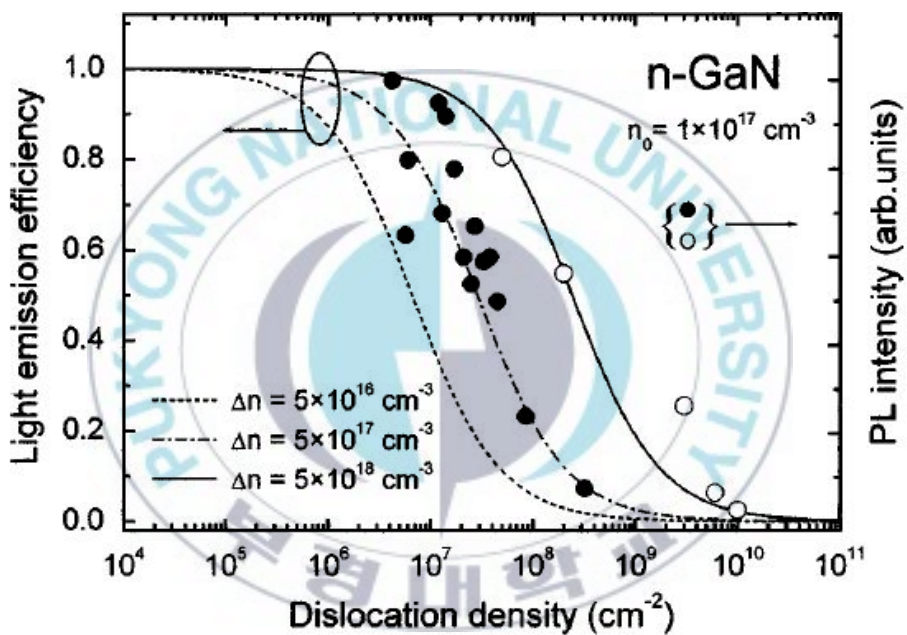


Figure 1.8. Light emission efficiency in GaN calculated for different nonequilibrium carrier concentrations (lines, left-hand side axis) and the PL intensity (circles, right-hand side axis) as a function of dislocation density. [24]

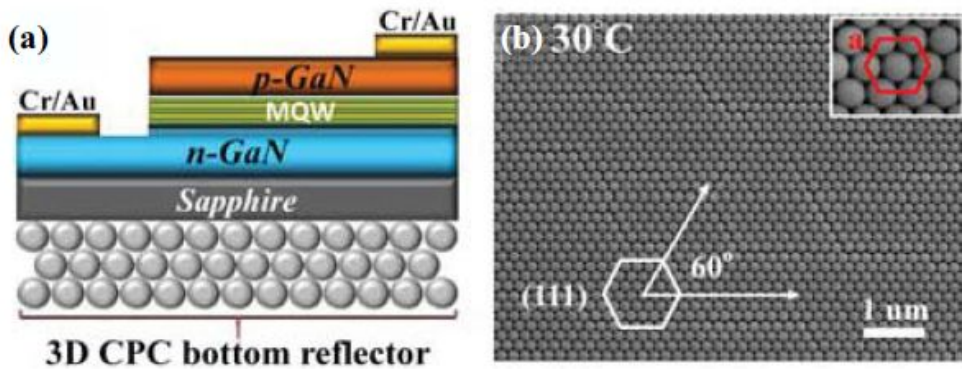


Figure 1.9. (a) Schematic LED structure with the 3-D- colloidal-phonic-crystal bottom reflector proposed in our study. (b) SEM surface images of colloidal-phonic-crystals fabricated at 30 °C show that the spheres stack with a well-organized (111) plane and fcc structure. Inset: lattice constant of colloidal-phonic-crystal is equivalent to the diameter of polystyrene sphere of 193 nm. [30]

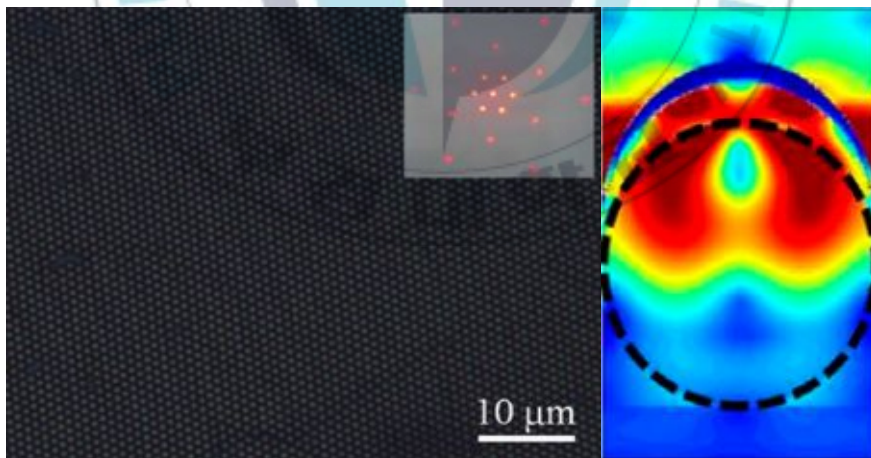


Figure 1.10. (left) Optical microscopy photo of the fabricated colloidal crystal monolayer and (right) its simulation result. [31]

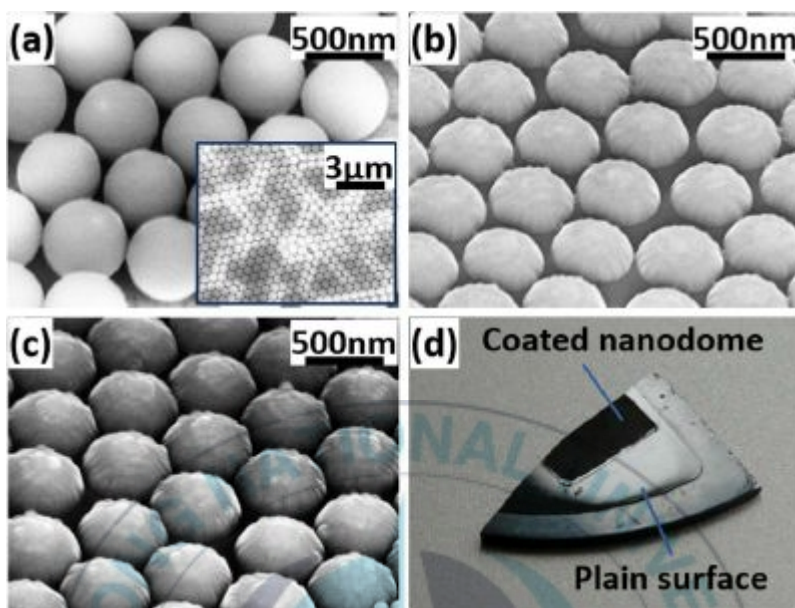


Figure 1.11. (left) Oblique-view SEM images of the (a) monolayer hexagonal close-packed polystyrene nanospheres (inset is a large-scale view), (b) fabricated SiC nanodome structures, and (c) Si₃N₄ coated nanodome structures respectively. (d) A photograph of SiC sample with a partially plain surface (lower right part) and partially covered by the coated nanodome structures (upper left part). [33]

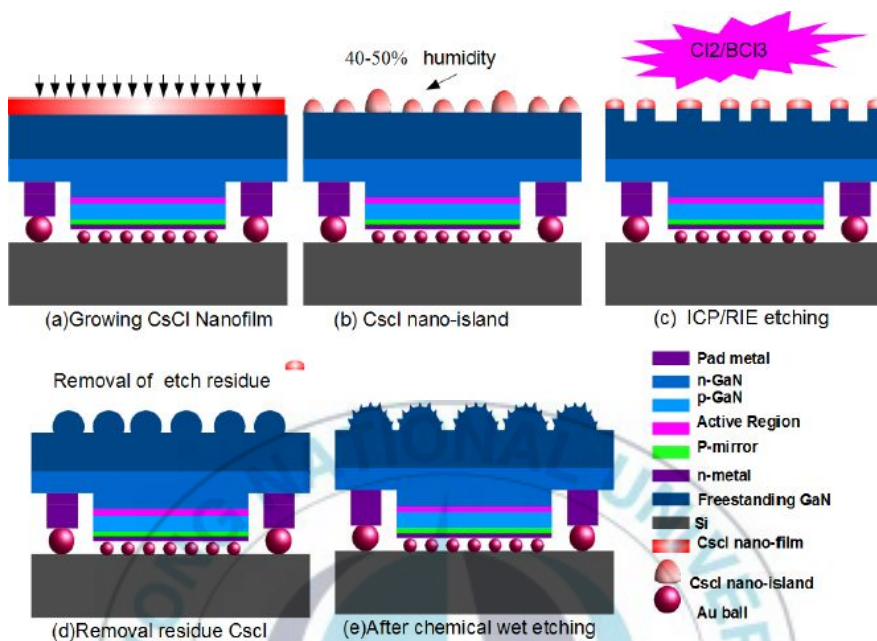


Figure 1.12. Schematic diagrams of fabrication process for nanotextured freestanding flip-chip LEDs. [36]

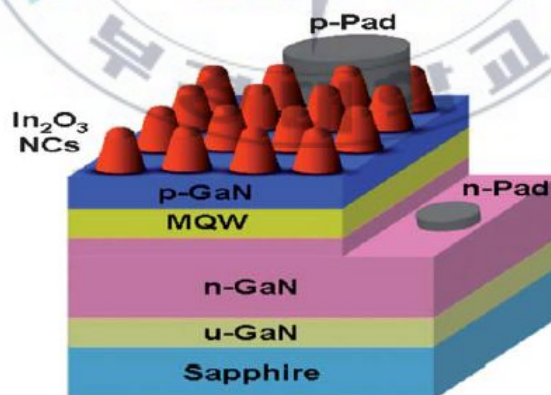


Figure 1.13. Cross-sectional scheme of an In_2O_3 nano-cones films/GaN-based LED. [38]

Recently, the fabrication of polymer nanolens arrays by tip-based nanolithography (dip-pen nanolithography) has been reported ³⁹. According to this report, poly(ethylene glycol) (PEG) lenses can be mass fabricated on any surface with a thin hydrophobic layer coating. In addition, the dimension of the PEG lenses can be conveniently controlled during the fabrication process; because the size of the PEG lens can be controlled by changing the AFM holding time on the substrate ³⁹. Besides the polymer nanostructures fabricated on a substrate, Zirconia (ZrO_2) nanoparticles (NPs) patterning in a large area was also reported ⁴⁰. The large scaled patterns of ZrO_2 NPs were obtained using a wettability tuning based lithography process: using polydimethylsiloxane (PDMS) stamp with hydrophobic material (mercaptohexadecanoic acid, MHA) and hydrophilic material (octadecanethiol, ODT). Using the reported lithography methods, a PEG nanolens array and ZrO_2 NPs can be applied onto GaN LED as materials for light extraction. These dip-pen nanolithography and PDMS-stamping-based micro/nanostructures fabricated for enhancement of LEE of GaN LED are away from the dislocation of the GaN layer that occurs by a chemical process, because micro/nanostructures will be directly placed onto a GaN LED with periodic order by mechanical method such as dip-pen nanolithography.

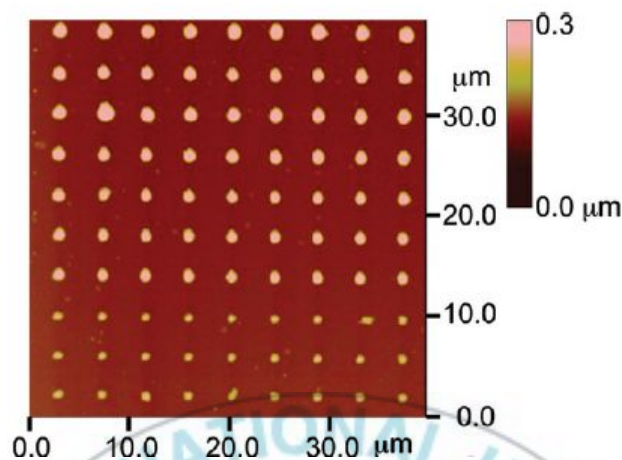


Figure 1.14. Tapping mode AFM topographic image of the PEG nanoscale lenses generated by dip-pen nanolithography. Lens size is dependent upon tip-substrate dwell time: 15 s (top row), 10 s (2nd to 4th row), 5 s (5th to 7th row), and 1 s (8th to 10th row). The PEG MW was 100000 Da. [39]

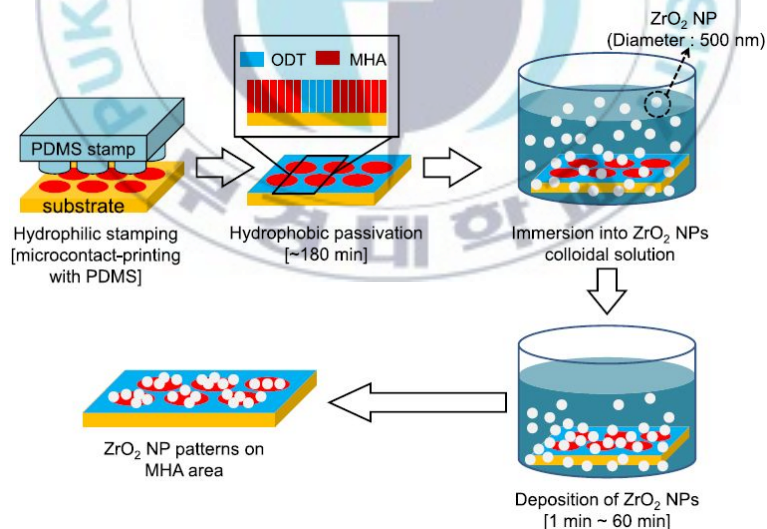


Figure 1.15. Scheme of procedure of ZrO_2 NP patterning with a wettability tuning method. [40]

In this paper, we investigate that enhancement of LEE in GaN LEDs by addressing wavelength-scaled PEG and ZrO₂ materials by means of three dimensional (3-D) finite-difference time-domain (FDTD) simulation experiments. Based upon favorably empirical approaches, hexagonal closed packed (*hcp*) arrays of PEG plano-convex lens (hemispherical), PEG and ZrO₂ particles (perfectly spherical) were considered as the nanostructures on GaN LED in the FDTD simulations. In particular, differently from the previous LEE studies using subwavelength-scaled materials^{14,27,37,38}, we investigate that the effect of LEE is graphically presented by the light profile demonstration LEDs, as well as the LEE is quantitatively calculated by light intensity analysis. In the results, the effect on the enhancement of LEE by the optical refractive index of the nanostructures is dominant in over-wavelength-scaled nanostructures addressed GaN LED, while there is no remarkable enhancement of LEE in subwavelength-scaled nanostructures addressed GaN LEDs. In the case of addressing similar-sized nanomaterials with the wavelength in the nanomaterials, the structural factor of the array of the nanomaterials is distinguishable in the intensity plots of the Poynting vector of GaN LEDs. Remarkably, by means of a ZrO₂ particle array ($\phi = 500$ nm) on top of the GaN LED, light extraction along the normal axis of the GaN LED surface is improved about six-fold symmetric pattern compared to a GaN LED structure without the extraction layer.

II. Experimental section

To measure the LEE of a multiple quantum well (MQW) GaN LED with the nanomaterials, 3-D FDTD simulation of electromagnetic (EM) wave was carried out with a commercial Maxwell's equation solver (FDTD Solution, Lumerical Inc.) using conformal mesh refinement method. The FDTD method is one of a kind of finite-element method to solve Maxwell's equation, it follows Yee's algorithm (see Figure 2.1). A schematic diagram of the 3-D FDTD simulation, which was carried out in this study, is shown in Figure 1. The MQW GaN LED ($16\ \mu\text{m} \times 16\ \mu\text{m} \times 2.6\ \mu\text{m}$: length \times width \times thickness) is set with a $2\ \mu\text{m}$ thick n -GaN layer, $0.1\ \mu\text{m}$ thick MQW layer, $0.2\ \mu\text{m}$ thick p -GaN layer, and Ag mirror of $0.3\ \mu\text{m}$ thickness [Figure 1(a)]. The refractive indices of vacuum and GaN were set as 1 and 2.47, respectively. For the MQW layer, 2.47 (GaN) and 2.52 (InGaN) were used as the refractive indices of the layer.

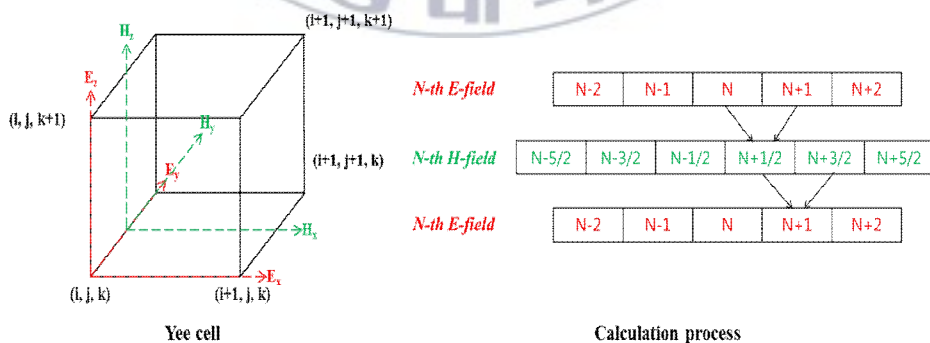


Figure 2.1. Yee algorithm to yield E-field and H-field

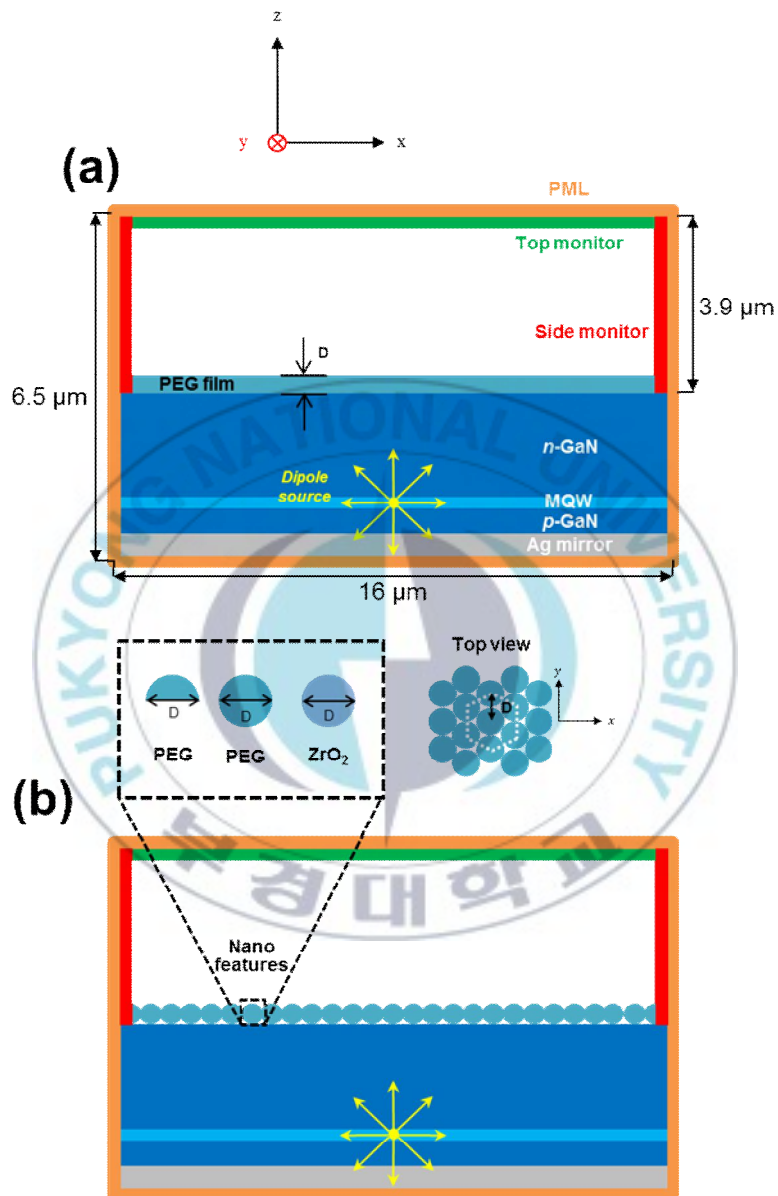


Figure 2.2. Schemes for 3-D FDTD simulation structures of (a) PEG film and (b) lens or particle addressed GaN LED.

In this study, we only limited the category of nanomaterials based upon the possibility of empirical fabrication of the nanofeatures; a PEG lens array can be addressed on top of a GaN LED by dip-pen nanolithography ³⁹, PEG and ZrO₂ particles are possibly self-assembled on top of GaN LED by a lithographic approach (wettability tuned patterning) ^{40,41}. The nanomaterials were put on top of the MQW GaN LED; *hcp* arrays of nanomaterials were considered as a layer for enhancing LEE [Figure 2.2(b)]. As a control experiment, PEG film was also considered in 3-D FDTD simulation [Figure 2.2(a)]. A single dipole source was placed in the middle of the MQW layer. The wavelength of the dipole source was set at 466 nm, and the oscillation direction of the dipole source was parallel to the *y*-axis, as shown in Figure 2.2(a). In addition, the transverse electric (TE) polarized dipole source is used for the FDTD calculation, due to the geometry of the MQW structure ¹⁹. The 3-D FDTD simulation region was set as 16 μm (*x*) × 16 μm (*y*) × 6.5 μm (*z*), surrounded by perfect matched layers (uniaxial PML), as displayed in Figure 2.2. In order to have accurate simulation reflected by the nanomaterials, the more number of Yee cells were placed in the region of the nanomaterials than the other regions; more than 5.0×10^7 number of Yee cells was set in the nanomaterials, whereas around 2.0×10^8 Yee cells were used in the other regions of the FDTD simulation. A plane monitor was placed at the top of the 3-D FDTD simulation region (the top monitor in Figure 2.2), where the top monitor is placed on the top *xy* plane of the simulation region. Two parallel couples of plane monitors were also positioned as the side monitors, as shown in Figure 2.2. The Poynting vector at the monitors with

different sizes of nanomaterials were measured for LEE calculation; D is the diameter of PEG lens, ZrO_2 particle, and PEG particle, while D is the thickness in the case of PEG film. The 3-D FDTD simulation was conducted with different D values: 100 nm, 200 nm, 300 nm, 400 nm, and 500 nm.



II. Results and Discussion

3.1. LEE enhancement

Figure 3.1 shows the enhancement of the LEE along the normal axis of GaN LED surface by the nanomaterials, by addressing the light extraction layer. The enhancement of LEE along the normal axis of the GaN LED surface is determined using the transmittance of the EM wave at the top monitor (T_{Top}) [see Figure 2.2 and the inset of Figure 3.1]. Then, the T_{Top} of the GaN LEDs with the nanomaterials is normalized by the T_{Top} of GaN LED without any light extraction layer (bare GaN LED) [$T_{\text{Top(GaN)}}$]. The normalized enhancement of the LEE along the normal axis of the GaN LED surface [$T_{\text{Top}}/T_{\text{Top(GaN)}}$] depending on the D of the nanomaterials is displayed in Figure 3.1. PEG film-addressed GaN LED shows a similar LEE to that of the bare GaN LED, and no remarkable change of $T_{\text{Top}}/T_{\text{Top(GaN)}}$ is observed as the thickness of the PEG film increases. For GaN LEDs with the light extraction layers using the nanomaterials, a similar value of $T_{\text{Top}}/T_{\text{Top(GaN)}}$ (~ 1) as that of the PEG film-addressed GaN LED is observed in the subwavelength-scaled nanomaterials (100 nm and 200 nm), regardless of the

type of nanomaterial. It means that the form factor of the nanomaterials is not distinguishable in subwavelength ($< 466 \text{ nm}$)-scaled nanomaterials addressed GaN LEDs.



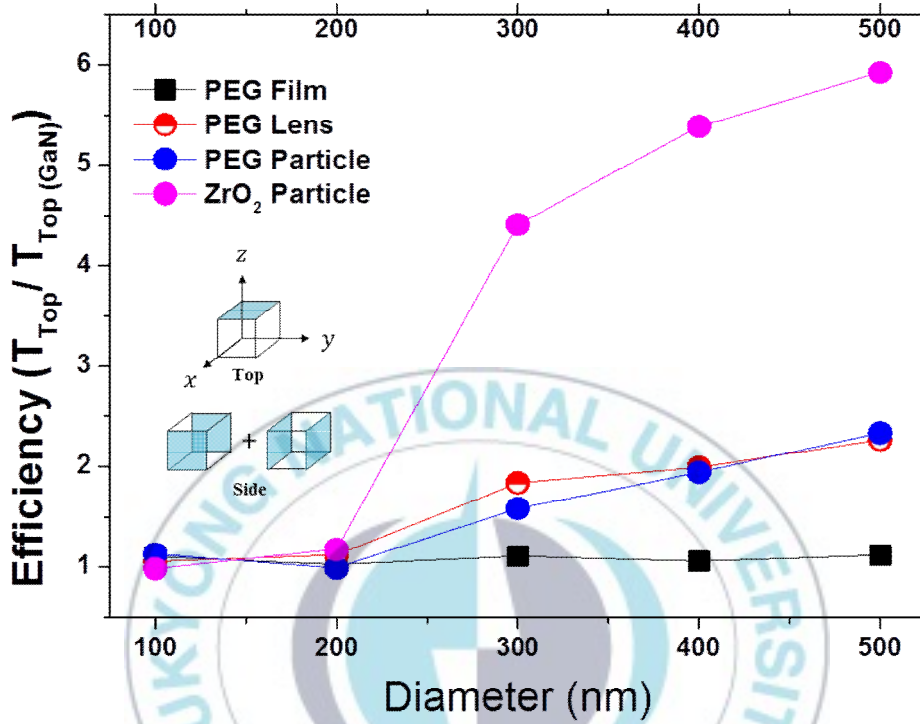
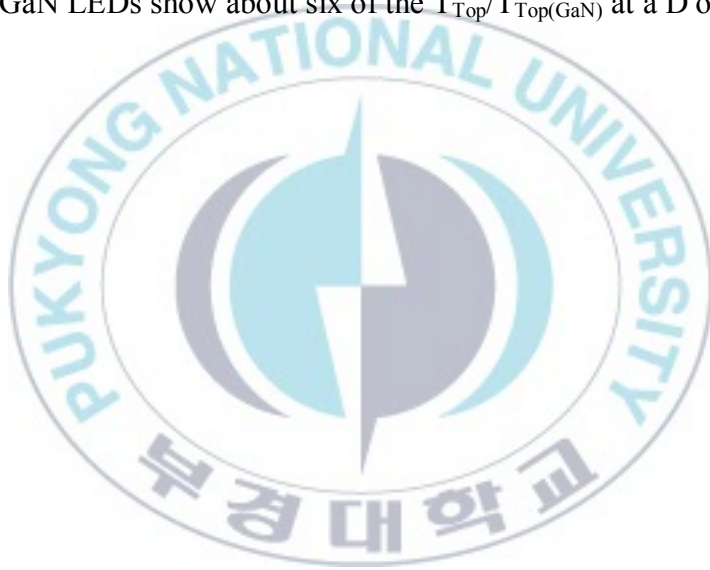


Figure 3.1. Normalized enhancement of LEE along the normal axis of the GaN LED surface.

On the other hand, there are observable changes of the $T_{\text{Top}}/T_{\text{Top(GaN)}}$ depending on D and the refractive index (n) of the nanomaterials in over-wavelength region (D : 300 nm, 400 nm, and 500 nm). First, the value of $T_{\text{Top}}/T_{\text{Top(GaN)}}$ in PEG lens and PEG particles slightly increases as D increases from 300 nm to 500 nm, keeping similar values in-between the PEG lens and the PEG particles addressed LEDs. Second, high-refractive-indexed ZrO_2

particle ($n_{\text{ZrO}_2} = 2.13$)⁴² addressed GaN LEDs show a larger $T_{\text{Top}}/T_{\text{Top(GaN)}}$ than PEG nanomaterials ($n_{\text{PEG}} = 1.47$)⁴³ addressed GaN LEDs. These observations mean that the effect by refractive index is more dominant than the effect by the form factor of the nanomaterials in the GaN LEDs with over-wavelength scaled nanomaterials. Interestingly, the ZrO_2 particle addressed GaN LEDs show about six of the $T_{\text{Top}}/T_{\text{Top(GaN)}}$ at a D of 500 nm.



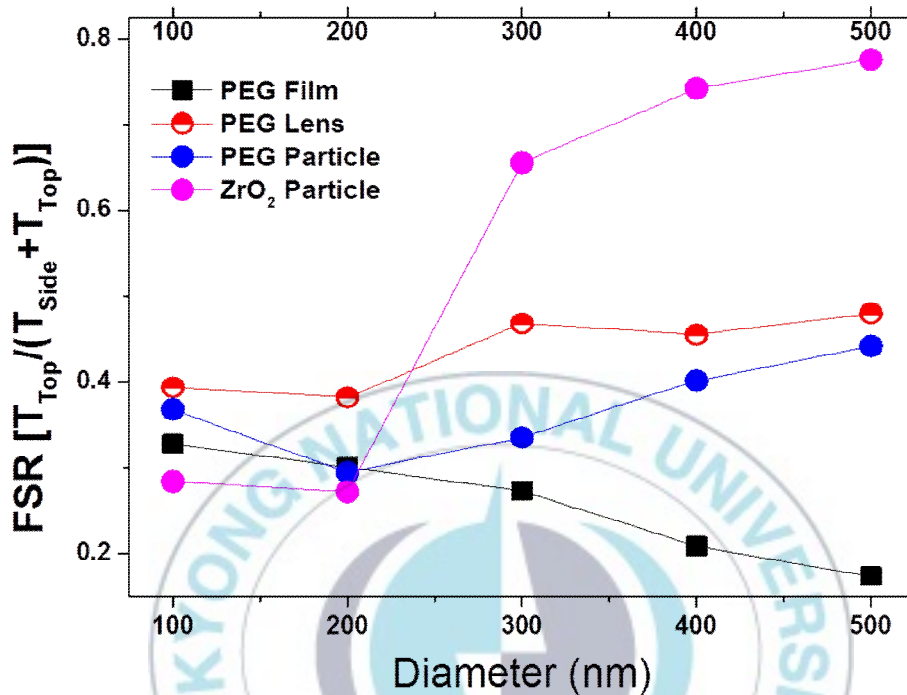


Figure 3.2.1 The top monitor transmittance ratio of the nanomaterials addressed GaN LEDs.

The top monitor transmittance ratio of the light extraction layer transmitted light from the nanomaterials addressed GaN LED was determined by $T_{\text{Top}}/(T_{\text{Side}} + T_{\text{Top}})$, where T_{Side} is sum of the transmittance of EM waves at the side, as shown in Figure 2.2 and the inset of Figure 3.1. Figure 3.2 represents the top monitor transmittance ratio $[T_{\text{Top}}/(T_{\text{Side}} + T_{\text{Top}})]$ of the GaN LED with different D of the nanomaterials. A bare GaN LED device shows

0.41 of $T_{\text{Top}}/(T_{\text{Side}} + T_{\text{Top}})$, as shown by the dark grey dotted lines in Figure 3.2.1

Most LEDs, except over-wavelength sized (≥ 300 nm) PEG lens and ZrO_2 addressed GaN LEDs, show less $T_{\text{Top}}/(T_{\text{Side}} + T_{\text{Top}})$ than that of bare GaN LEDs; this means that the subwavelength-scaled nanomaterials strengthen transmittance to the sides by scattering, that is hampering $T_{\text{Top}}/(T_{\text{Side}} + T_{\text{Top}})$, in the GaN LEDs. The PEG film addressed GaN LED shows that $T_{\text{Top}}/(T_{\text{Side}} + T_{\text{Top}})$ decreases as D (thickness) increases; the EM wave bypassed to the side monitors is more grown with a thicker PEG film. Therefore, decreasing the $T_{\text{Top}}/(T_{\text{Side}} + T_{\text{Top}})$ can be related with the development of the bypassed EM wave in the PEG film as the PEG film gets thicker. In the case of subwavelength-scaled (100 nm and 200 nm) PEG lenses, PEG particle and ZrO_2 particle addressed GaN LEDs, $T_{\text{Top}}/(T_{\text{Side}} + T_{\text{Top}})$ slightly decreases as D increases from 100 nm to 200 nm, as shown in Figure 3.2.1

On the other hand, for the $T_{\text{Top}}/(T_{\text{Side}} + T_{\text{Top}})$ of over-wavelength-scaled (300 nm, 400 nm, and 500 nm) PEG lens, PEG particle, and ZrO_2 particle addressed GaN LEDs show an increment as D increases. This is because Mie scattering becomes stronger as the particle size is similar or over to wavelength of incident light. The $T_{\text{Top}}/(T_{\text{Side}} + T_{\text{Top}})$ of particles

and lens addressed GaN LEDs also tends to increase in this region of D . In detail, the $T_{\text{Top}}/(T_{\text{Side}} + T_{\text{Top}})$ of the PEG lens addressed GaN LEDs increase from 0.38 ($D = 200$ nm) to 0.48 ($D = 500$ nm). For PEG particle addressed GaN LED, a minimum value of $T_{\text{Top}}/(T_{\text{Side}} + T_{\text{Top}})$ is shown at a D of 200 nm (0.30), and increases to 0.44 as D increases to 500 nm. The value of the $T_{\text{Top}}/(T_{\text{Side}} + T_{\text{Top}})$ of PEG lens addressed GaN LEDs is larger than that of PEG particle addressed for the same D . The thickness of the layer of the PEG lens array is exactly half the thickness of the layer of the PEG particle array [definition of “ D ” in Figure 2.2(b)]. In the case of equivalent D , a PEG lens addressed GaN LED will have a lesser ratio of bypassed EM wave to the side of the light extraction layer than PEG particle addressed GaN LED. In case of a ZrO_2 particle addressed GaN LED, $T_{\text{Top}}/(T_{\text{Side}} + T_{\text{Top}})$ slightly decreases from 0.28 to 0.27 when D increases from 100 nm to 200 nm, and $T_{\text{Top}}/(T_{\text{Side}} + T_{\text{Top}})$ increases to 0.78 as D increases to 500 nm. Over-wavelength-sized ZrO_2 particle addressed GaN LEDs show a larger value for $T_{\text{Top}}/(T_{\text{Side}} + T_{\text{Top}})$ than the others.

Figure 3.2.2(a) and S1(b) represent the $|P_{xz}|$ and $|P_{yz}|$ of bare GaN LED, respectively. $|P_{xy}|$ and $|P_{Far}|$ of bare GaN LED are also respectively shown in Figure 3.2.2(c) and S1(d). The

$|P_{xz}|$, $|P_{yz}|$, $|P_{xy}|$, and $|P_{Far}|$ of bare GaN LED are very similar as those of subwavelength-sized ($D = 100$ nm and 200 nm) PEG film addressed GaN LEDs. Interestingly, the low intensity Poynting vectors are shown at the middle of GaN LED in $|P_{xz}|$, $|P_{yz}|$, $|P_{xy}|$, and $|P_{Far}|$. It can be understood that the interference effect by the Ag mirror is emphasized in this geometry of GaN LED ($2\text{ }\mu\text{m}$ thick n -GaN layer, $0.1\text{ }\mu\text{m}$ thick MQW layer, $0.2\text{ }\mu\text{m}$ thick p -GaN layer, and $0.3\text{ }\mu\text{m}$ thick Ag mirror).



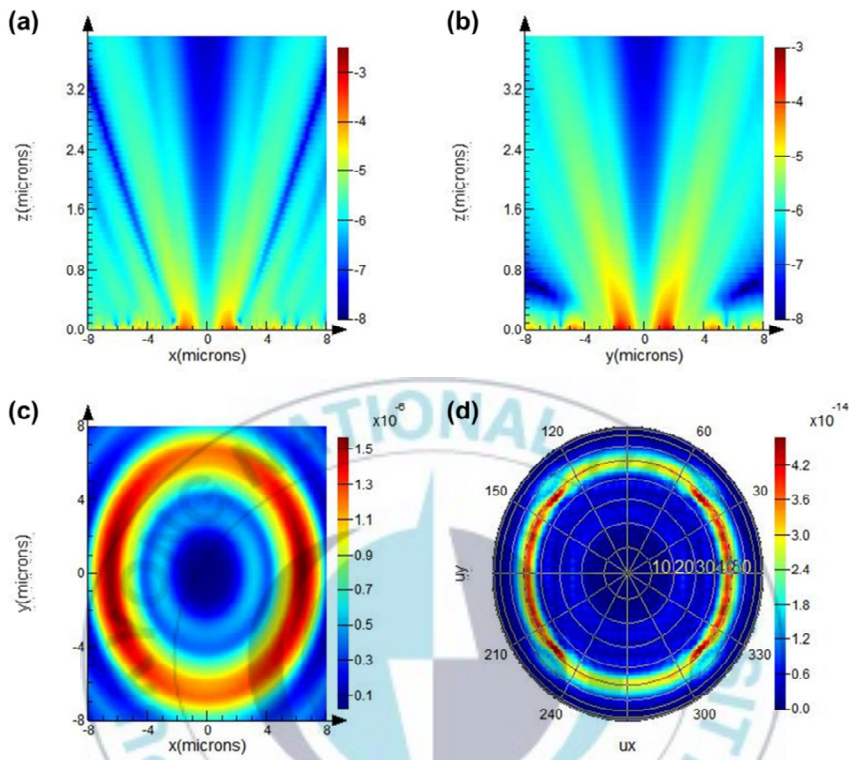


Figure 3.2.2. $|P_{xz}|$ and $|P_{yz}|$ of bare GaN LED: (a) xz -view (at $y = 0$) and (b) yz -view (at $x = 0$) of intensity (log scale) of Poynting vector above GaN layer of the bare GaN LED. The intensity at the (c) top monitor ($|P_{xy}|$) and (d) far-field distribution ($|P_{Far}|$) of the Poynting vector in bare GaN LED PEG film. The numbers inside the far-field graph denote the polar angle of the far-field hemisphere.

3.2. Poynting vector intensity: xz view above the GaN layer

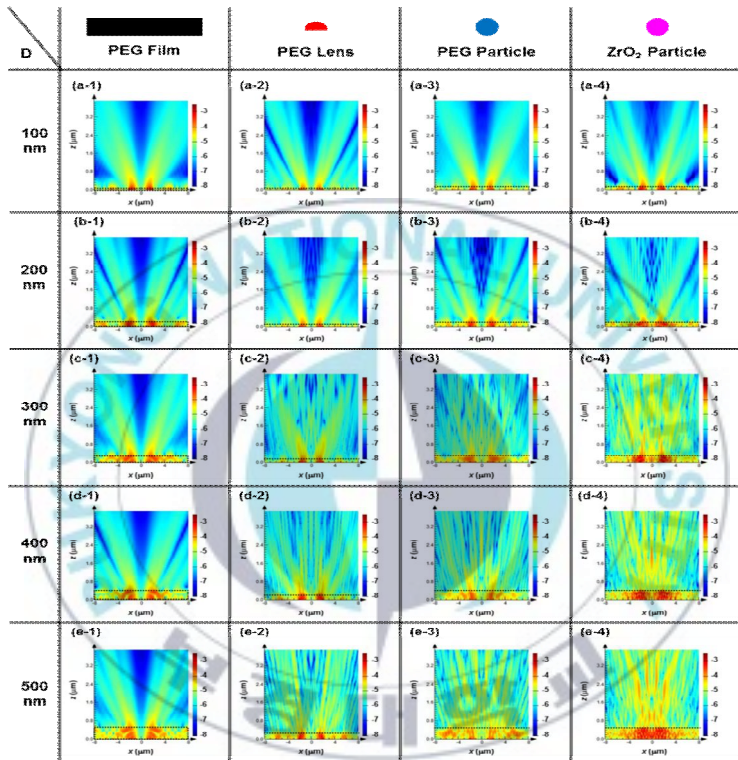


Figure 3.3.1. $|P_{xz}|$: xz -view (at $y = 0$) of intensity (log scale) of Poynting vectors above the GaN layer of the nanomaterials addressed LEDs. (a) $D = 100$ nm, (b) 200 nm, (c) 300 nm, (d) 400 nm, and (e) 500 nm. Tier of 1, 2, 3, and 4 represent the PEG film, PEG lens, PEG particle, and ZrO_2 particle addressed GaN LEDs, respectively. The black dotted lines represent the layer of nanomaterials-placed region.

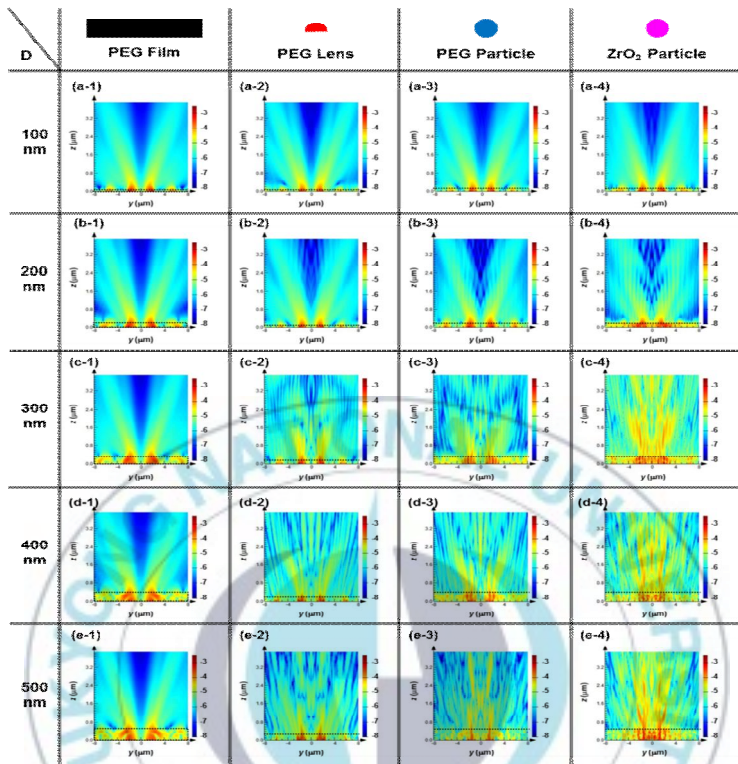


Figure 3.3.2. $|P_{yz}|$: yz-view (at $x = 0$) of intensity (log scale) of the Poynting vectors above the GaN layer of the nanomaterials addressed LEDs. (a) $D = 100$ nm, (b) 200 nm, (c) 300 nm, (d) 400 nm, and (e) 500 nm. Tier of 1, 2, 3, and 4 represent the PEG film, PEG lens, PEG particle, and ZrO_2 particle addressed GaN LEDs, respectively. The black dotted lines represent the layer of nanomaterials placed region.

In order to investigate the scattering of light by the light extraction layers, the xz-view (at $y = 0$) intensity of Poynting vector above the GaN layer ($|P_{xz}|$) in the nanomaterials addressed LEDs are shown in Figure 3.3.1. As a guide, the

layer of nanomaterials placed region is marked by black dotted lines. In the case of subwavelength-sized nanomaterials ($D = 100 \text{ nm}$ and 200 nm) addressed GaN LEDs, $|P_{xz}|$ shows a relatively similar profile. When D is 100 nm , the $|P_{xz}|$ shows two strongly scattered rays close to $x = 0$ in all the GaN LEDs. For 100 nm ZrO_2 particles addressed GaN LEDs, an additional two strongly scattered rays are shown beside the two strongly scattered rays close to $x = 0$. When D is 200 nm , the $|P_{xz}|$ still shows the two strongly scattered rays in the center; however, interference-pattern-like branches are shown in the particles and lens addressed GaN LEDs, while no interference-pattern is shown in the PEG film addressed GaN LED. In Figure 3.3.1(a), the $|P_{xz}|$ of 100 nm ZrO_2 particles addressed GaN LEDs shows that more rays and branches go through the sides than that of the other 100 nm nanomaterials addressed GaN LEDs. Moreover, the $|P_{xz}|$ of 200 nm ZrO_2 particles addressed GaN LEDs shows more interference patterns than that of the other 100 nm nanomaterials addressed GaN LEDs, as shown in Figure 3.3.1(b), which are reflected in Figure 3.1 as having the lowest $T_{\text{Top}}/(T_{\text{Side}} + T_{\text{Top}})$ of the 100 nm and 200 nm ZrO_2 particles addressed GaN LEDs. More scattering and interferences could be obtained by high-refractive-indexed

ZrO₂ particles than other subwavelength-scaled nanomaterials (100 nm and 200 nm) cases. For the PEG-film addressed GaN LED, more rays and branches of $|P_{xz}|$ are pass through the sides guided by the PEG films as D increases, which is well matched with the reduced $T_{\text{Top}}/(T_{\text{Side}} + T_{\text{Top}})$ in Figure 3.2.1 While the relatively similar profiles of $|P_{xz}|$ are shown in subwavelength-sized nanomaterials (D = 100 nm and 200 nm) addressed GaN LEDs, the $|P_{xz}|$ profiles of over-wavelength-sized particles and lenses addressed GaN LEDs show strong scattering and interference-like patterns, as displayed in Figure 3.3.1(c), 3(d), and 3(e). Remarkably, 500 nm ZrO₂ particles addressed GaN LED show the most higher intensity (red color) rays and branches in $|P_{xz}|$ profile, and the largest $|P_{xz}|$ in the layer of nanomaterials; accordingly, the maximum (~ 6) value of $T_{\text{Top}}/T_{\text{Top(GaN)}}$ is also shown here.

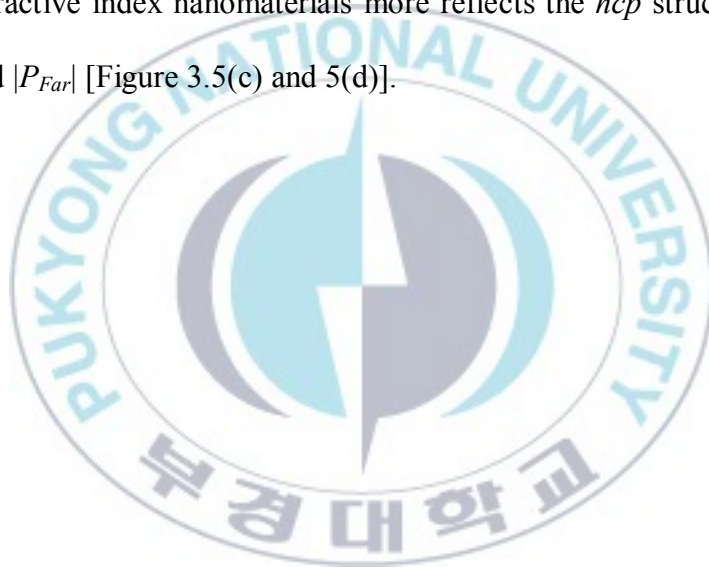
3.3. Poynting vector intensity: xy view and far-field

To examine the light scattering in xy distribution, the intensity of the Poynting vector at the top monitor (see Figure 2.2), $|P_{xy}|$, of the nanomaterials addressed LEDs was obtained by FDTD simulation. In addition, the far-field distribution of the Poynting vector ($|P_{Far}| \approx |E_{Far}|^2$) in the nanomaterials addressed LEDs was also FDTD simulated. Figure 3.4 shows the $|P_{xy}|$ and $|P_{Far}|$ of the subwavelength-scaled nanomaterials ($D = 100$ nm) addressed GaN LEDs; (a), (b), (c), and (d) represent the PEG film, PEG particle, PEG lens, and ZrO_2 particle addressed GaN LED, respectively. It can be expected that the maximum of $|P_{xy}|$ and $|P_{Far}|$ on the x -axis ($y = 0$) is larger than that on the y -axis ($x = 0$) in Figure 3.4, owing to the direction of the dipole source oscillation. Interestingly, a similar “O” shaped pattern of $|P_{xy}|$ is shown in all the LEDs, which well matches with the similar $|P_{xz}|$ shown in Figure 3.3.1(a); likewise, the $|P_{xy}|$ and $|P_{Far}|$ in Figure 3.4 display a similar “O” shaped pattern with four-fold symmetry. It is assumed that the four-fold symmetry in $|P_{Far}|$ originates from the square shape of the GaN LED device in the xy plane ($16 \mu\text{m} \times 16 \mu\text{m}$). In particular, the 100 nm ZrO_2 particle addressed GaN LED [Figure 3.4(d)] shows more ripples in the “O”

shaped patterns of $|P_{xy}|$ and $|P_{Far}|$, as well as a more obvious doubled “O” shape pattern in $|P_{Far}|$ than the others [Figure 3.4(a), 4(b), and 4(c)]. This means that 100 nm ZrO_2 particles scatter more light than the other 100 nm nanomaterials; which well corresponds with the lowest $T_{\text{Top}}/(T_{\text{Side}} + T_{\text{Top}})$ in Figure 3.2.1.

In Figure 3.5, the nanomaterials-dependent $|P_{xy}|$ and $|P_{Far}|$ patterns are shown in 200 nm nanomaterials addressed GaN LEDs. While 200 nm PEG film addressed GaN LED shows no distinguishable changes in $|P_{xy}|$ and $|P_{Far}|$ [Figure 3.5(a)], 200 nm PEG lens addressed GaN LEDs have somehow changed $|P_{xy}|$ and $|P_{Far}|$ from the “O” shape by scattering and interference effects, as displayed in Figure 3.5(b). On the other hand, the $|P_{xy}|$ and $|P_{Far}|$ of 200 nm PEG and ZrO_2 particle addressed GaN LEDs show more changes (patterns by scattering and interference) in Figure 3.5(c) and 5(d). In particular, a six-fold symmetry (hexagonal pattern) appears in both Figure 3.5(c) and 5(d). The six-fold symmetry for the $|P_{xy}|$ and $|P_{Far}|$ patterns seems to reflect the *hcp* structure of the nanomaterials’ light extraction layers. The degree of change in the $|P_{xy}|$ and $|P_{Far}|$ of the PEG lens addressed GaN LED is weaker than that of PEG and ZrO_2 particle addressed GaN LEDs. This

indicates that the thicker light extraction layer composed of nanomaterials has more effect on the change in $|P_{xy}|$ and $|P_{Far}|$; the thickness of the layer of the 200 nm PEG lens array is 100 nm. The 200 nm ZrO_2 particle addressed GaN LED shows more change in $|P_{xy}|$ and $|P_{Far}|$ than in the case of 200 nm PEG particle addressed GaN LED; a light extraction layer composed of the higher refractive index nanomaterials more reflects the *hcp* structural factor to $|P_{xy}|$ and $|P_{Far}|$ [Figure 3.5(c) and 5(d)].



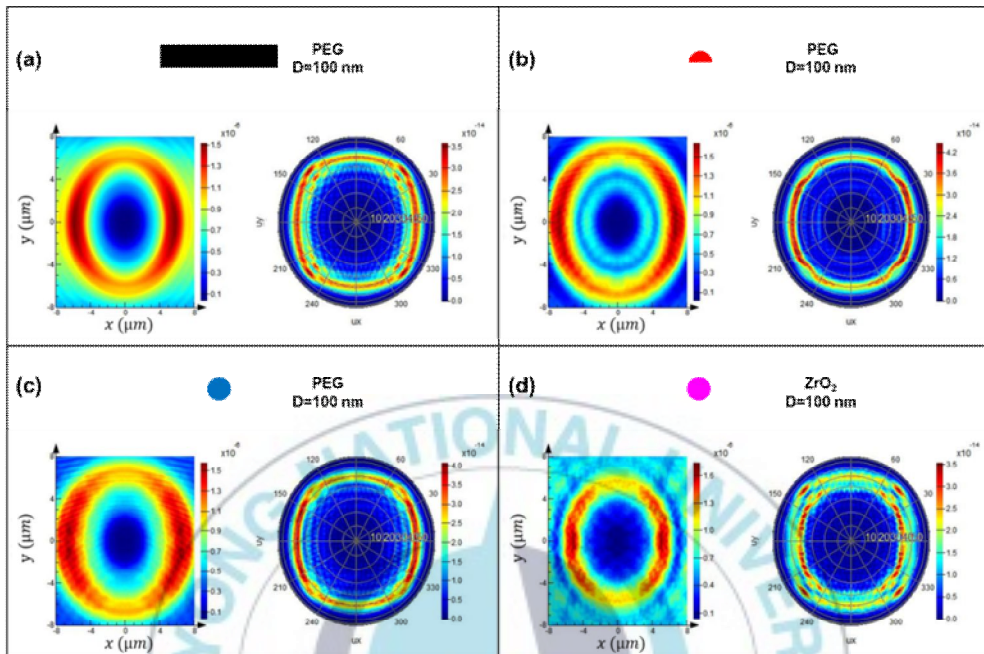


Figure 3.4. Intensity at the top monitor ($|P_{xy}|$, left) and far-field distribution ($|P_{Far}|$, right) of Poynting vector in (a) PEG film, (b) PEG lens, (c) PEG particle, and (d) ZrO_2 particle nanomaterials addressed LEDs with $D = 100$ nm. The numbers inside of the far-field graph denote the polar angle of the far-field hemisphere.

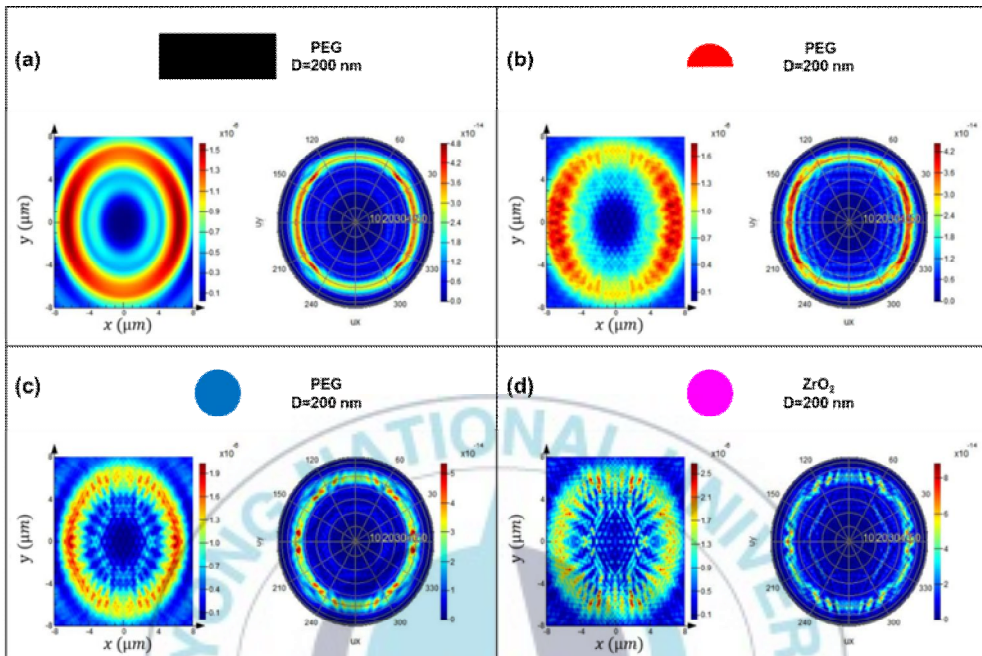


Figure 3.5. Intensity at the top monitor ($|P_{xy}|$, left) and far-field distribution ($|P_{Far}|$, right) of the Poynting vector in (a) PEG film, (b) PEG lens, (c) PEG particle, and (d) ZrO_2 particle nanomaterials addressed LEDs with $D = 200\text{nm}$. The numbers inside the far-field graph denote the polar angle of the far-field hemisphere.

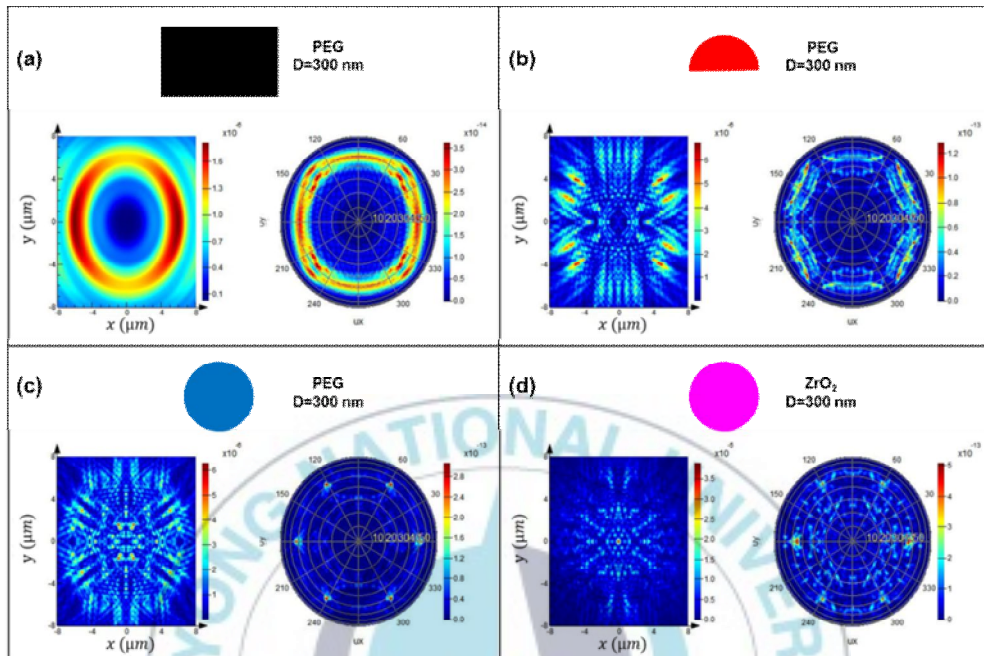


Figure 3.6.1. Intensity at the top monitor ($|P_{xy}|$, left) and far-field distribution ($|P_{Far}|$, right) of Poynting vector in (a) PEG film, (b) PEG lens, (c) PEG particle, and (d) ZrO_2 particle nanomaterials addressed LEDs with $D = 300\text{ nm}$. The numbers inside the far-field graph denote the polar angle of the far-field hemisphere.

Figure 3.6.1 shows that the $|P_{xy}|$ and $|P_{Far}|$ of nanomaterials addressed GaN LEDs in the case of $D = 300\text{ nm}$. The similar “O” shaped pattern shown in Figure 3.4(a) and 5(a) is also obtained in 300 nm PEG film addressed GaN LEDs [Figure 3.6.1(a)]. However, remarkably distinguishable six-fold

symmetry is observed in Figure 3.6.1(b), 6(c), and 6(d). And Figure 3.6.2 shows the $|P_{xy}|$ and $|P_{Far}|$ of the 400 nm nanomaterials addressed GaN LEDs, and $|P_{xy}|$ and $|P_{Far}|$ of the 500 nm nanomaterials addressed GaN LEDs are shown in Figure 3.6.3. In the case of the lens and particles addressed GaN LEDs, the patterns of six-fold symmetry that originates from the *hcp* structural factor are shown in $|P_{xy}|$ and $|P_{Far}|$ patterns, similar to Figure 3.6.1.



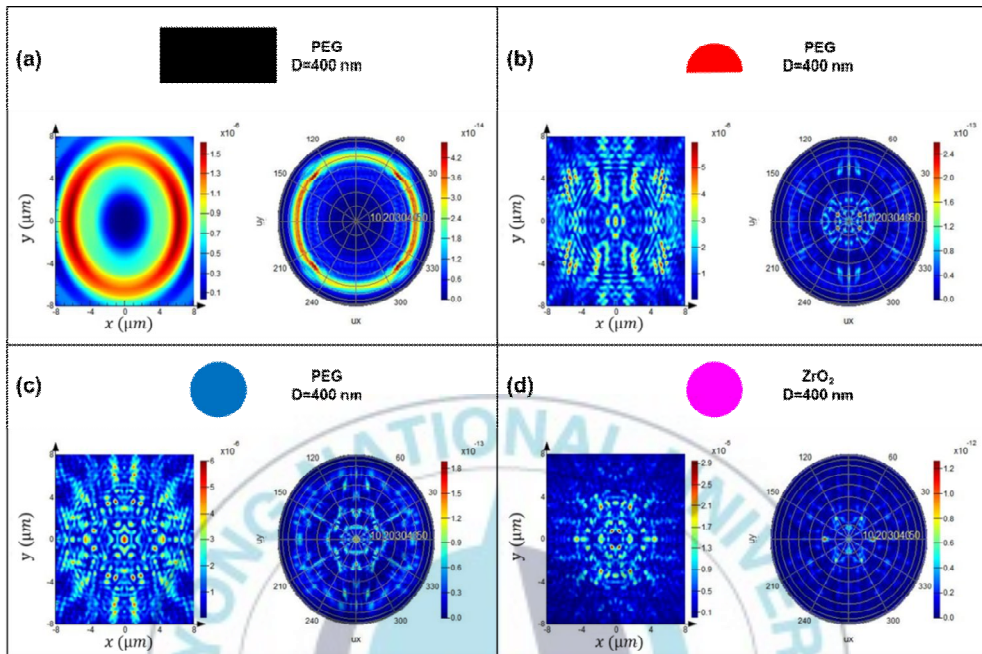


Figure 3.6.2. Intensity at the top monitor ($|P_{xy}|$, left) and far-field distribution ($|P_{Far}|$, right) of the Poynting vector in (a) PEG film, (b) PEG lens, (c) PEG particle, and (d) ZrO_2 particle nanomaterials addressed LEDs with $D = 400$ nm. The numbers inside the far-field graph denote the polar angle of the far-field hemisphere.

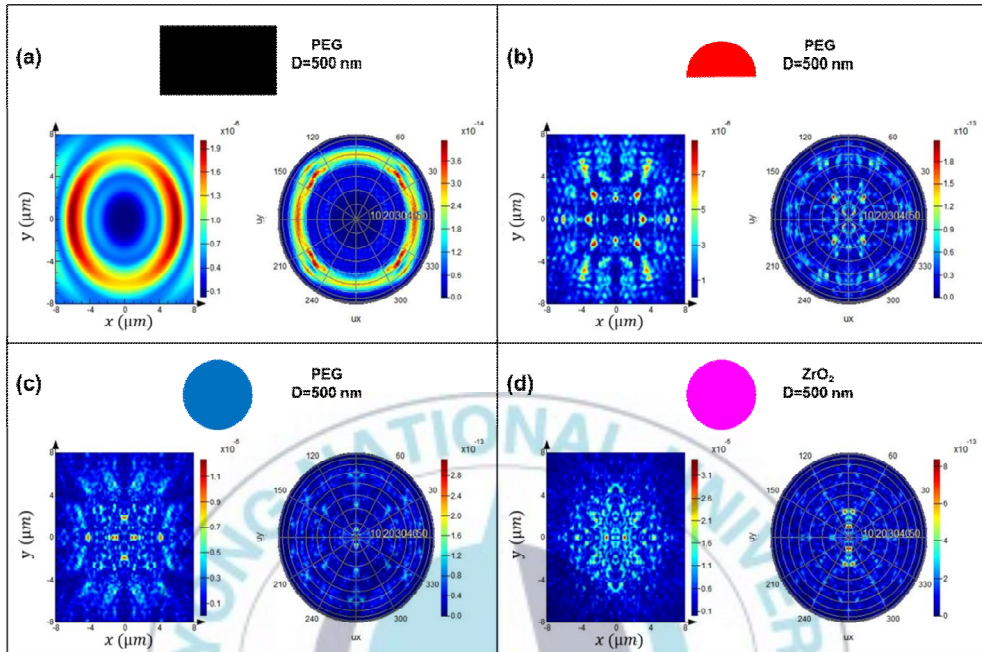


Figure 3.6.3. Intensity at the top monitor ($|P_{xy}|$, left) and far-field distribution ($|P_{Far}|$, right) of Poynting vector in (a) PEG film, (b) PEG lens, (c) PEG particle, and (d) ZrO_2 particle nanomaterials addressed LEDs with $D = 500$ nm. The numbers inside of the far-field graph denote the polar angle of the far-field half sphere.

It can be understood that hcp structural factor reflected $|P_{xy}|$ and $|P_{Far}|$ patterns become more remarkable as D increases from 200 nm to 300 nm. Our results prove that the structural factor of the light extraction layer becomes remarkable when the size of nanomaterials is larger than the λ_{Eff} of

the nanomaterials. The effective wavelength (λ_{Eff}) of the irradiant light (466 nm) in PEG and ZrO_2 materials will be changed into 317 nm and 219 nm, respectively, following Snell's law: $\lambda_{\text{Eff}} = (466 \text{ nm})/n$.



IV. Conclusion

Light extraction of the empirically obtainable nanomaterials addressed GaN LEDs is successfully demonstrated by means of 3-D FDTD simulation. In the results, several straightforward factors can be proven through scrutinizing the distributions of Poynting vector intensity. It can be summarized that 1) Subwavelength scaled nanomaterials addressed GaN LEDs show similar light extraction behaviors: $T_{\text{Top}}/T_{\text{Top(GaN)}}$, $|P_{xz}|$, $|P_{xy}|$ and $|P_{\text{Far}}|$. 2) For over-wavelength scaled nanomaterials addressed GaN LEDs, light extraction resulting from scattering and interference is more efficient by refractive index than by the shape of the nanomaterials: The higher $T_{\text{Top}}/(T_{\text{Side}} + T_{\text{Top}})$ and more rays and branches of $|P_{xz}|$ in ZrO_2 addressed GaN LEDs. 3) The structural factor of the light extraction layer becomes remarkable when the size of nanomaterials is larger than λ_{Eff} : the six-fold symmetry of the $|P_{xy}|$ and $|P_{\text{Far}}|$. 4) Remarkably, LEE is up to 5.92 for 500 nm ZrO_2 particles addressed GaN LED: Mie scattering and interference seem to be strengthened by the light extraction layer of increasing ZrO_2 particles with *hcp* structure in over-wavelength scale.

Our investigation can give a speculation on “light–matter” subwavelength interaction, including shape and dielectric effects. Moreover, the LEE of GaN LED can be empirically improved, based upon our results.

V. Reference

- ¹ S. Nakamura, Adv. Mater. (Weinheim, Ger.) **8**, 689 (1996).
- ² H. W. Huang, J. K. Huang, C. H. Lin, K. Y. Lee, H. W. Hsu, C. C. Yu, and H. C. Kuo, IEEE Electron Device Lett. **31**, 582 (2010).
- ³ J. H. Son, B. J. Kim, C. J. Ryu, Y. H. Song, H. K. Lee, J. W. Choi, and J.-L. Lee, Opt. Express **20**, A287 (2012).
- ⁴ M.-K. Kwon, J.-Y. Kim, I.-K. Park, K. S. Kim, G.-Y. Jung, S.-J. Park, J. W. Kim, and Y. C. Kim, Appl. Phys. Lett. **92**, 251110/1 (2008).
- ⁵ L.-W. Jang, J.-W. Ju, D.-W. Jeon, J.-W. Park, A. Y. Polyakov, S.-J. Lee, J.-H. Baek, S.-M. Lee, Y.-H. Cho, and I.-H. Lee, Opt. Express **20**, 6036 (2012).
- ⁶ P. Zhu, G. Liu, J. Zhang, and N. Tansu, J. Disp. Technol. **9**, 317 (2013).
- ⁷ B. U. Ye, B. J. Kim, J. Park, H. Y. Jeong, J. Y. Park, J. K. Kim, J.-H. Hur, M. H. Kim, J.-L. Lee, and J. M. Baik, Adv. Funct. Mater. **24**, 3384 (2014).
- ⁸ H.-W. Huang, C. F. Lai, W. C. Wang, T. C. Lu, H. C. Kuo, S. C. Wang, R. J. Tsai, and C. C. Yu, Electrochem. Solid-State Lett. **10**, H59 (2007).
- ⁹ Y. Jin, F. Yang, Q. Li, Z. Zhu, J. Zhu, and S. Fan, Opt. Express **20**, 15818 (2012).
- ¹⁰ W. J. Choi, Q. H. Park, D. Kim, H. Jeon, C. Sone, and Y. Park, J. Korean Phys. Soc. **49**, 877 (2006).
- ¹¹ S.-Y. Jung, J. Choe, M.-S. Seok, Q. H. Park, and T.-Y. Seong, Mater. Sci. Semicond. Process. **16**, 582 (2013).
- ¹² Y. C. Shin, D. H. Kim, E. H. Kim, J.-M. Park, K.-M. Ho, K. Constant, J. H. Choe, Q. H. Park, H.-Y. Ryu, J. H. Baek, T. Jung, and T. G. Kim, IEEE J. Quantum Electron. **46**, 116 (2010).

- ¹³ Y. M. Song, E. S. Choi, G. C. Park, C. Y. Park, S. J. Jang, and Y. T. Lee, *Appl. Phys. Lett.* **97**, 093110/1 (2010).
- ¹⁴ F. W. Mont, J. K. Kim, M. F. Schubert, E. F. Schubert, and R. W. Siegel, *J. Appl. Phys.* **103**, 083120/1 (2008).
- ¹⁵ P. T. Chung, C. T. Yang, S. H. Wang, C. W. Chen, A. S. T. Chiang, and C.-Y. Liu, *Mater. Chem. Phys.* **136**, 868 (2012).
- ¹⁶ Y. Ou, D. D. Corell, C. Dam-Hansen, P. M. Petersen, and H. Ou, *Opt. Express* **19**, A166 (2011).
- ¹⁷ C.-H. Sun, P. Jiang, and B. Jiang, *Appl. Phys. Lett.* **92**, 061112/1 (2008).
- ¹⁸ Y. Kanamori, M. Okochi, and K. Hane, *Opt. Express* **21**, 322 (2013).
- ¹⁹ P. Zhao and H. Zhao, *Opt. Express* **20**, A765 (2012).
- ²⁰ T. N. Oder, K. H. Kim, J. Y. Lin, and H. X. Jiang, *Appl. Phys. Lett.* **84**, 466 (2004).
- ²¹ M. F. Schubert, S. Chhajed, J. K. Kim, E. F. Schubert, D. D. Koleske, M. H. Crawford, S. R. Lee, A. J. Fischer, G. Thaler, and M. A. Banas, *Appl. Phys. Lett.* **91**, 231114/1 (2007).
- ²² T. Hikosaka, H. Yoshida, N. Sugiyama, and S. Nunoue, *Phys. Status Solidi C* **11**, 617 (2014).
- ²³ Q. Dai, M. F. Schubert, M. H. Kim, J. K. Kim, E. F. Schubert, D. D. Koleske, M. H. Crawford, S. R. Lee, A. J. Fischer, G. Thaler, and M. A. Banas, *Appl. Phys. Lett.* **94**, 111109/1 (2009).
- ²⁴ S. Y. Karpov and Y. N. Makarov, *Appl. Phys. Lett.* **81**, 4721 (2002).
- ²⁵ W. Smigaj, B. Gralak, R. Pierre, and G. Tayeb, *Opt Lett* **34**, 3532 (2009).
- ²⁶ C.-Y. Huang, H.-M. Ku, and S. Chao, *Opt. Express* **17**, 23702 (2009).
- ²⁷ K. H. Li and H. W. Choi, *J. Appl. Phys.* **110**, 053104/1 (2011).

- ²⁸ T. Wei, K. Wu, D. Lan, Q. Yan, Y. Chen, C. Du, J. Wang, Y. Zeng, and J. Li, *Appl. Phys. Lett.* **101**, 211111/1 (2012).
- ²⁹ K.-M. Huang, H.-J. Chang, C.-L. Ho, and M.-C. Wu, *IEEE Photonics Technol. Lett.* **24**, 1298 (2012).
- ³⁰ E. K. Kang, Y. M. Song, S. J. Jang, C. I. Yeo, and Y. T. Lee, *IEEE Photonics Technol. Lett.* **25**, 1118 (2013).
- ³¹ Z.-q. Liu, X.-s. Liu, G.-q. Liu, H.-b. Shao, and J. Chen, *Mater. Lett.* **126**, 224 (2014).
- ³² Z. Q. Liu, G. Q. Liu, J. Chen, Y. Hu, X. N. Zhang, and Z. J. Zheng, *Mater. Lett.* **116**, 382 (2014).
- ³³ Y. Ou, X. Zhu, V. Jokubavicius, R. Yakimova, N. A. Mortensen, M. Syvajarvi, S. Xiao, and H. Ou, *Sci. Rep.* **4** (2014).
- ³⁴ Y.-H. Cheng, J.-L. Wu, C.-H. Cheng, K.-C. Syao, and M.-C. M. Lee, *Appl. Phys. Lett.* **90**, 091102/1 (2007).
- ³⁵ J. H. Kang, J. H. Ryu, H. K. Kim, H. Y. Kim, N. Han, M. S. Lee, Y. J. Park, P. Uthirakumar, V. V. Lysak, and C.-H. Hong, *Thin Solid Films* **520**, 437 (2011).
- ³⁶ B. Sun, L. Zhao, T. Wei, X. Yi, Z. Liu, G. Wang, J. Li, and F. Yi, *Opt. Express* **20**, 18537 (2012).
- ³⁷ H. W. Huang, C. H. Lin, C. C. Yu, K. Y. Lee, B. D. Lee, H. C. Kuo, S. Y. Kuo, K. M. Leung, and S. C. Wang, *Mater. Sci. Eng., B* **151**, 205 (2008).
- ³⁸ J.-T. Lian, J.-H. Ye, J.-Y. Liou, K.-C. Tsao, N.-C. Chen, and T.-Y. Lin, *J. Mater. Chem. C* **1**, 6559 (2013).
- ³⁹ J.-W. Jang, Z. Zheng, O.-S. Lee, W. Shim, G. Zheng, G. C. Schatz, and C. A. Mirkin, *Nano Lett.* **10**, 4399 (2010).
- ⁴⁰ M.-S. Yang, S.-J. Son, B. C. Park, B. K. Moon, and J.-W. Jang, *J. Appl. Phys. (Melville, NY, U. S.)* **114**, 234306/1 (2013).

- ⁴¹ J. H. Park, S. Hwang, and J. Kwak, *Langmuir* **27**, 8548 (2011).
- ⁴² Haynes, W.M., Ed. CRC Press/Taylor and Francis: Boca Raton, FL, CRC Handbook of Chemistry and Physics, 93rd Edition.
- ⁴³ H. El-Kashef, *Physica B* **279**, 295 (2000)

